JCI insight

TRPC1 links calcium signaling to cellular senescence in the protection against post-traumatic osteoarthritis

Meike Sambale, … , Thomas Pap, Joanna Sherwood

JCI Insight. 2024. https://doi.org/10.1172/jci.insight.182103.

Research In-Press Preview Bone biology Cell biology

Graphical abstract

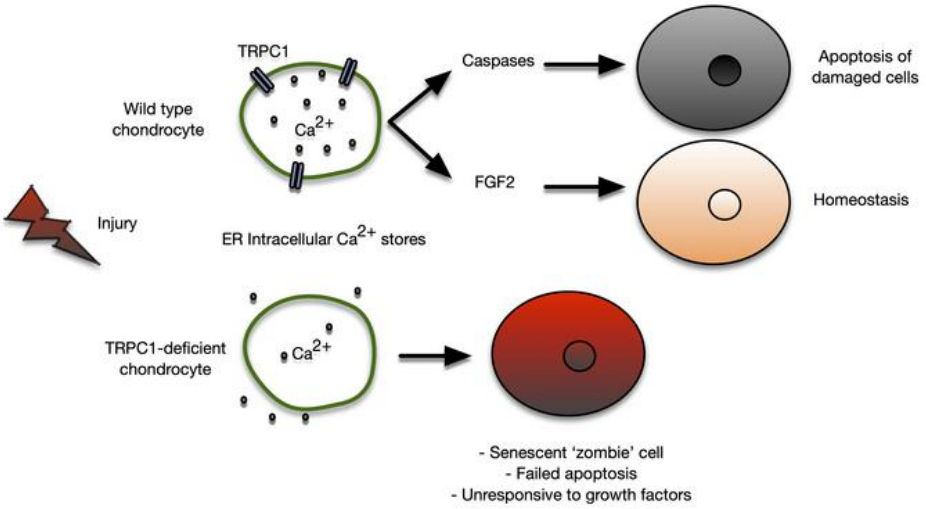

TRPC1 links calcium signaling to cellular senescence in the protection against post-traumatic osteoarthritis

Meike Sambale[1], Starlee Lively[2], Osvaldo Espin-Garcia[2,3], Pratibha Potla[2], Chiara Pastrello[2], Sarah Bödecker[1], Linda Wessendorf[1], Simon Kleimann[1], Peter Paruzel[1], Rojiar Asgarian[1], Alexandra Tosun[1], Johanna Intemann[1], Jessica Bertrand[4], Francesco Dell'Accio[5], Mohit Kapoor[2], Thomas Pap[1], Joanna Sherwood[1].

[1] Institute of Musculoskeletal Medicine, University Hospital Münster, Münster, Germany

[2] Osteoarthritis Research Program, Division of Orthopaedics, Schroeder Arthritis Institute, University Health Network, and Krembil Research Institute, University Health Network, Toronto, Ontario, Canada.

[3] Department of Epidemiology and Biostatistics, University of Western Ontario, London, Ontario, Canada; Dalla Lana School of Public Health and Department of Statistical Sciences, University of Toronto, Toronto, Ontario, Canada; Department of Biostatistics, University Health Network, Toronto, Ontario, Canada

[4] Department of Orthopaedic Surgery, Otto-von-Guericke University Magdeburg, Magdeburg, Germany.

[5] Experimental Medicine and Rheumatology, Queen Mary University of London, London, United Kingdom.

Corresponding Author

Dr. Joanna Sherwood
Institute of Musculoskeletal Medicine,
University Hospital Münster, Domagkstrasse
3, 48143 Münster
Germany. +49 251 8356757
sherwood@uni-muenster.de

Disclosure Statement

The authors have declared that no conflict of interest exists.

Abstract

Transient receptor potential channel 1 (TRPC1) is a widely expressed mechanosensitive ion channel located within the endoplasmic reticulum membrane, crucial for refilling depleted internal calcium stores during activation of calcium-dependent signaling pathways. Here, we have demonstrated that TRPC1 activity is protective within cartilage homeostasis in the prevention of cellular senescence associated cartilage breakdown during mechanical and inflammatory challenge. We revealed that TRPC1 loss is associated with early stages of osteoarthritis (OA) and plays a non-redundant role in calcium signaling in chondrocytes. *Trpc1*$^{-/-}$ mice subjected to destabilization of the medial meniscus induced OA developed a more severe OA phenotype than wild type controls. During early OA development, *Trpc1*$^{-/-}$ mice displayed an increased chondrocyte survival rate, however remaining cells displayed features of senescence including p16^{INK4a} expression and decreased Sox9. RNA sequencing identified differentially expressed genes related to cell number, apoptosis and extracellular matrix organization. *Trpc1*$^{-/-}$ chondrocytes exhibited accelerated dedifferentiation, while demonstrating an increased susceptibility to cellular senescence. Targeting the mechanism of TRPC1 activation may be a promising therapeutic strategy in osteoarthritis prevention.

Keywords

Calcium signaling, cartilage, chondrocytes, cellular senescence, osteoarthritis

Introduction

Osteoarthritis (OA) is a chronic degenerative joint disorder featuring severe destruction of the articular cartilage, subchondral bone remodeling and localized inflammation that causes pain, disability, and reduced quality of life to millions of people worldwide (1, 2). No approved disease modifying osteoarthritis drug (DMOAD) options are currently available; and so OA progression is first managed via the administration of NSAIDs and physiotherapy, before ultimately resorting to joint arthroplasty. Loss of chondrocyte phenotypic stability is a hallmark of OA development, whereby the chondrocytes situated within the cartilage extracellular matrix (ECM) ultimately fail in their compensatory expression of key anabolic markers such as Sox9 and type II collagen, and increase their expression of hypertrophic and catabolic markers such as inflammatory cytokines, type X collagen and matrix metalloproteinases (MMPs) (3, 4).

The involvement of ion channels in OA-mediated processes has been identified, and yet the role of such channels and their mechanisms of activity remain understudied in OA research (5). Disregulation of calcium signaling pathways resulting in alterations to local electrostatic fields and protein synthesis (6) has been implicated to lead to increased expression of catabolic enzymes including MMP13, alongside an increase in cell death (7, 8). Controlled oscillation of intracellular Ca^{2+} concentrations is a highly conserved phenomenon found in many different cell types. They are required for modulating downstream gene expression profiles and various cellular processes, including those involved in maintaining a stable chondrocyte phenotype through the regulation of expression of key genes including Sox9 and aggrecan (9, 10). Transient receptor potential canonical 1 (TRPC1) channel is a broadly expressed member of the TRP superfamily of cation channels that is normally situated within the endoplasmic reticulum (ER) membrane. TRPC1 channels can form heteromeric complexes with other TRP channels or with stromal interaction molecule (STIM) and

Orai, key players in store-operated calcium entry (SOCE) (11, 12). Activation upon mechanical or receptor driven depletion of intracellular Ca^{2+} stores leads to activation of STIM1, which in turn activates TRPC1 and Orai1 channels to allow influx of extracellular Ca^{2+} into the cell, driving the controlled Ca^{2+} oscillation cycles.

While cyclic shear and compressive forces are required for normal articular cartilage development and homeostasis (13), OA is exacerbated by the increased force exerted on cartilage following biomechanical alterations and early disease associated matrix changes. Mechanical stimulation generated from cyclic forces, for example during typical weight bearing movement, stimulates repeated Ca^{2+} influx activity within the chondrocytes (14). Activation of mechanoreceptors in chondrocytes including TRPV4 and PIEZO2 has been demonstrated to trigger anabolic and homeostatic responses, demonstrating the potential for ion channels to be targeted within the search for potential DMOAD therapies (15-17). While little is known about the specific role of TRPC1 in chondrocytes, deficiency of *Trpc1* in mice has been observed to limit skeletal muscle contraction during sustained activity suggesting that TRPC1 may be required to sufficiently and repeatedly refill intracellular stores during prolonged stimulation (18).

Here we investigate the hypothesis that TRPC1 plays a functional role within cartilage homeostasis during the refilling of intracellular Ca^{2+} stores required to maintain controlled intracellular Ca^{2+} oscillations triggered by biomechanical and biochemical signaling in the joint. We examine how OA development influences the expression of TRPC1, and how the loss of TRPC1 leads to reduced chondrocyte phenotypic stability and increased cartilage damage within the destabilization of the medial meniscus (DMM) model of surgically induced OA. Our data suggest that the loss of TRPC1 during early OA predisposes the cartilage to an increased cellular senescence linked phenotype triggered by both mechanical and inflammatory challenge

Results

TRPC1 is expressed in human and murine articular cartilage, is reduced during OA development and is functionally non-redundant.

TRPC channels are known to mediate an intracellular Ca^{2+} response to mechanical force, therefore considering the role of mechanical stress as a predominant driver in OA development, we compared the expression of TRPC channels in OA patients within a previously published microarray set (GSE114007) (19). At mRNA level, *TRPC1* was the most highly expressed TRPC channel in both normal and OA cartilage (Supplemental Figure 1A).

We hypothesized that TRPC1 is required in chondrocytes during the refilling of intracellular Ca^{2+} stores following and during activation of signaling pathways. In order to assess how the lack of TRPC1 affects the ability to respond to biochemical stimuli known to drive intracellular Ca^{2+} release, intracellular calcium measurements were collected before and following addition of stimuli, such as thapsigargin, to wild type and *Trpc1*$^{-/-}$ chondrocytes using a Fluo-4 fluorescent intracellular indicator (Figure 1A). Wild type and *Trpc1*$^{-/-}$ chondrocytes were crucially found to have an equal level of intracellular calcium mobilization in resting conditions (Figure 1B). PBS, used as a control for the mechanical disturbance caused by the addition of liquid into the resting medium, did not produce a release of intracellular calcium in either genotype (Supplemental Figure 2). In contrast, ionomycin, an ionophore known to facilitate the transfer of Ca^{2+} into cells led to an increase in intracellular calcium in both genotypes, however this mobilization was tempered significantly in *Trpc1*$^{-/-}$ chondrocytes compared to in controls (Figure 1C). Thapsigargin, an inhibitor of endoplasmic reticulum ATPase Ca^{2+} pumps, causes Ca^{2+} to be released from intracellular stores

(20). Stimulation of wild type chondrocytes led to a relatively long-lived increase in intracellular calcium, however this again appears stunted in *Trpc1*$^{-/-}$ chondrocytes (Figure 1D). bFGF, a physiological stimuli involved in mechanically-induced biochemical signaling in chondrocytes (21) drove an increase in intracellular Ca^{2+} concentrations in wild type cells, which was found to be significantly lower in *Trpc1*$^{-/-}$ chondrocytes (Figure 1E). This analysis demonstrates that the function of TRPC1 cannot be fully compensated for, suggesting that TRPC1 is an important and non-redundant channel in chondrocytes.

Immunofluorescence staining for TRPC1 in wild type murine chondrocytes before and following bFGF stimulation demonstrated the relocation of TRPC1 channels from the endoplasmic reticulum to the cell surface, where they are expected to contribute to the influx of Ca^{2+} (Figure 1F) (22). In cartilage tissue, TRPC1 protein expression was examined using immunohistochemical staining of paraffin sections of human knee articular cartilage from healthy and OA donors. While expression was evident in chondrocytes throughout the cartilage in samples from healthy joints, protein levels were reduced significantly between early stages and advanced stages of human OA disease (Figure 1G, H). A similar phenomenon was observed in mice, where expression in wild type murine knee joints was assessed in sham and DMM knees 2 weeks and 8 weeks following surgery. A reduced level of TRPC1 protein found within the articular cartilage at both early and later stages of OA development (Figure 1I, J).

By mining previously published datasets, we could show that *TRPC1* is downregulated at gene expression level by human chondrocytes *in vitro* by IL-1β as an inflammatory stimulus (GSE75181) (Supplemental figure 1B) as well as in cartilage explants following mechanical injury (Supplemental figure 1C) (23).

Trpc1 is required for articular cartilage homeostasis following DMM challenge.

To investigate the possible effects of a lack of TRPC1 expression, the knee joint structure and cartilage phenotype of *Trpc1*-deficient mice were compared to wild type controls. No developmental anomalies were found during examination of newborn murine knee joints (Supplemental Figure 3A), while the bodyweights, articular cartilage thickness and joint phenotype of unchallenged 10 week old mice were found to be equal to controls (Supplementary Figure 3B, C), indicating that the lack of TRPC1 does not lead to an altered phenotype during skeletal development. However, *Trpc1*$^{-/-}$ mice subjected to the DMM model of surgically induced joint instability were found to develop a more severe OA-like phenotype, as illustrated by an increased OARSI score assessment of cartilage defects 8 weeks following surgery (Figure 2A, B). This phenotype was accompanied by a decreased level of type II collagen staining within the articular cartilage of *Trpc1*$^{-/-}$ joints post-DMM, indicating an increased collagen matrix breakdown (Figure 2C, D). These findings indicate that the absence of TRPC1 exacerbates cartilage degradation observed 8 weeks after DMM surgery.

Early alterations in knee joint phenotype are evident in Trpc1$^{-/-}$ mice 2 weeks post-DMM

In order to analyze the role of TRPC1 during the early initiation phase of OA development, prior to significant structural damage to the articular surface, *Trpc1*$^{-/-}$ murine knee joints 2 weeks post- DMM were compared to wild type controls with histological analysis showing no obvious differences in articular cartilage structure (Figure 3A, B). MicroCT analysis of the tibial plateau at this timepoint demonstrated that whilst wild type controls begin to exhibit an increase in subchondral bone density including an increase in trabecular thickening, *Trpc1*$^{-/-}$ joints were slower to respond, if at all, to the alteration in joint biomechanics caused by the DMM (Figure 3C-E,

Supplemental Figure 4). These more subtle changes were accompanied by a reduction in type II collagen (Figure 3F, G), where a significant decrease in protein levels in DMM knees compared to sham controls was evident in *Trpc1*$^{-/-}$ murine knee articular cartilage but not in wild type. Similarly, a greater increase in type X collagen as a marker of chondrocyte hypertrophic differentiation was found in *Trpc1*$^{-/-}$ tibial cartilage following DMM than in wild type controls (Figure 3H, I), indicating that, when triggered by joint destabilization, the lack of TRPC1 may accelerate the phenotypic switch of articular chondrocytes to a more pathological state that results in the more pronounced cartilage breakdown visibly observed by OARSI scoring at 8 weeks post-DMM.

Development of a cellular senescent phenotype in Trpc1*$^{-/-}$ *articular cartilage following DMM

In order to further understand the chondrocyte phenotypic changes occurring 2 weeks post-DMM in the *Trpc1*$^{-/-}$ animals, cartilage sections were next assessed for Sox9 expression, a key promotor of chondrocyte differentiation (24). A comparable decline of Sox9-positive cells was observed in the cartilage of both wild type and *Trpc1*-deficient animals 2 weeks post-DMM compared to corresponding sham animals (Figure 4A, B). Remarkably however, while the absolute number of Sox9^{+} cells was reduced, the overall number of surviving DAPI^{+} cells within the same area was found to be significantly higher in *Trpc1*$^{-/-}$ cartilage than in that of wild type mice following DMM (Figure 4C), indicating that a large number of cells no longer expressing Sox9 remain within the articular cartilage of *Trpc1*$^{-/-}$ mice following OA induction. Next, Ki67 staining was used to assess whether the increased cellularity in *Trpc1*$^{-/-}$ cartilage reflected a higher proliferative rate of the remaining cells, however, although the absolute number of Ki67^{+} proliferating cells was higher in *Trpc1*$^{-/-}$ cartilage than in wild type, this increase was normalized by the overall increase in DAPI^{+} cellularity (Figure 4D-F), meaning that no overall increase was observed in the proliferation activity of the remaining cells at this timepoint. Similarly, although an assessment of active cell death using

TUNEL staining demonstrated more TUNEL^{+} cells within *Trpc1*$^{-/-}$ knee articular cartilage post-DMM, this difference was lost when normalized to the total number of cells remaining in the cartilage (Figure 4 G-I). Interestingly, an evaluation of the number of empty lacunae left within the tibial cartilage of wild type and *Trpc1*$^{-/-}$ mice 2 weeks post-DMM suggested that a lower rate of cell death may have occurred in *Trpc1*$^{-/-}$ mice at an earlier timepoint (Figure 4J), which may account for a higher overall cellularity at this stage. Notably, immunofluorescence staining demonstrated an increased expression of MMP13 within the articular cartilage of *Trpc1*$^{-/-}$ mice 2 weeks post- DMM (Figure 4K, L). These data suggest that TRPC1 may be necessary to regulate the survival rate of dedifferentiated chondrocytes during OA development and triggers the question of what role these additional remaining cells might be playing.

Expression profiles of murine cartilage and subchondral bone are altered in Trpc1*$^{-/-}$ *mice 2 weeks post-DMM

To gain further insight into the early pathogenic mechanisms causing the effects observed during OA development in the joints of *Trpc1*$^{-/-}$ animals, RNA sequencing was performed on femoral condyle and tibial plateau cartilage collected 2 weeks post-DMM from wild type and *Trpc1*$^{-/-}$ mice (Figure 5A). Up- and downregulated expression of all genes was first visualized on a volcano plot (Figure 5B). 294 significantly differentially expressed genes (DEGs), defined as logFC>1.5 and P_{adj}<0.05, were identified. The top 100 DEGs can be viewed within Supplemental Table 1. Next, hierarchical clustering of all genes with logFC>1.5 helped visualize expression variation among animals and highlight the consistent DMM-driven transcription profile that emerged in *Trpc1*$^{-/-}$ mice (Figure 5C). GO enrichment analysis identified the biological processes (BP) with the greatest distinctions between *Trpc1*$^{-/-}$ and WT animals (Figure 5D). Interestingly, and perhaps not surprisingly based on the findings presented so far, the top 6 enriched BP that emerged in *Trpc1*$^{-/-}$

animals were: 1) homeostasis of number of cells (GO:0048872); 2) regulation of apoptotic signaling pathway (GO:2001233); 3) cell-substrate adhesion (GO:0031589); and 4-6) organization of ECM and extracellular structures (GO:0043062, GO:0030198, GO:0031589).

TRPC1 deficiency leads to chondrocyte phenotypic instability and an increased susceptibility to cellular senescence

Given the differences shown in the RNAseq in the expression of genes related to cell homeostasis and extracellular matrix organization following DMM, we next examined the effect of the absence of TRPC1 on the phenotype of articular chondrocytes during in vitro passage. Key phenotypic genes were expressed at comparable high levels by freshly expanded chondrocytes taken from 4-6 day old wild type and *Trpc1*$^{-/-}$ unchallenged knee joints (Figure 6A-D), however during serial passage, which trials the ability of chondrocytes to maintain their phenotypic stability (25), a number of differences are apparent. Sox9 gene expression remained approximately equal between genotypes during passage (Figure 6A), however the expression of aggrecan and Col2a1 were significantly lower during passage in *Trpc1*$^{-/-}$ chondrocytes as compared to wild type controls (Figure 6B, C). Conversely, Col1a1 expression was significantly higher during passage of *Trpc1*$^{-/-}$ chondrocytes compared to controls (Figure 6D), indicating an accelerated dedifferentiation of the chondrocytes.

Cellular plasticity and senescence are complexly interlinked processes (26). To measure whether the accelerated dedifferentiation observed in *Trpc1*$^{-/-}$ chondrocytes was associated with the development of an altered senescent phenotype, wild type and *Trpc1*$^{-/-}$ chondrocytes were stained for β-galactosidase activity, an indicator of cellular senescence. Very little staining was observed in either genotype at P0, however an increased proportion of SA-β-Gal+ cells was observed during passage in *Trpc1*$^{-/-}$ chondrocytes compared to controls, indicating an accelerated differentiation towards a senescent fate (Figure 6E, F). Similarly, p16^{INK4a}, another marker of cellular senescence,

was found to be expressed at significantly higher levels in *Trpc1*$^{-/-}$ chondrocytes during passage than in controls at both RNA (Figure 6G) and at protein (Figure 6H, I) levels. Taken together, these findings indicate that in the absence of TRPC1, chondrocytes exhibit an accelerated differentiation towards a senescent fate *in vitro*.

Finally, we wanted to determine if TRPC1 deficiency influences whether chondrocytes shift towards a senescent phenotype following exposure to IL-1β as an inflammatory stimulus associated with OA disease pathogenesis (27, 28). Treatment with IL-1β led to an increase in the proportion of SA-β-Gal+ cells with a significantly higher rate of detection found in *Trpc1*$^{-/-}$ chondrocytes compared to wild types (Figure 7A, B). This effect was exacerbated when observed following further culture in IL-1β-free control medium for an additional 24 or 48 hours, indicating that once triggered, the inflammation-driven development of cellular senescence in *Trpc1*$^{-/-}$ chondrocytes may become chronic even without the presence of IL-1β. No differences were detected between the proliferation rates of *Trpc1*$^{-/-}$ chondrocytes cultured either in control or IL-1β treated conditions (Figure 7C). At protein level, a significantly higher amount of $p16^{INK4a}$ was detected in *Trpc1*$^{-/-}$ chondrocytes compared to wild type controls following IL-1β stimulation (Figure 7D, E) further indicating the development of a more senescence-like phenotype of *Trpc1*$^{-/-}$ cells following IL-1β exposure.

We then tested whether the *Trpc1*$^{-/-}$ chondrocytes exhibited any of the secretory phenotype characteristic of senescent cells. Interestingly, the SASP CCL-2 concentration was found to be significantly higher within the supernatant of IL-1β treated *Trpc1*$^{-/-}$ chondrocytes as compared to that of wild type controls (Figure 7F), although this was not the case for other SASPs including IL-6 and MMP3 (Supplemental Figure 5A, B). In order to understand the mechanism behind the increased cellularity observed in the *Trpc1*$^{-/-}$ osteoarthritic cartilage, we tested whether TRPC1 regulation of Ca^{2+} signaling, which is strictly required for caspase activity via cytochrome C (29), is required for caspase mediated apoptosis. Following exposure to IL-1β, *Trpc1*$^{-/-}$ chondrocytes were unable to

upregulate caspase activity indicating a failure to initiate and undergo apoptosis (Figure 7G, H).

These observations also left us with the question of whether chondrocyte senescence was altered in *Trpc1*$^{-/-}$ animals after DMM. Immunofluorescent staining analysis demonstrated that although the proportion of p16^{INK4a}-positive chondrocytes were comparable between wild type controls and *Trpc1*$^{-/-}$ following sham surgery, 2 weeks post-DMM the proportion of p16^{INK4a}-positive cells in *Trpc1*$^{-/-}$ cartilage was significantly higher (Figure 7I, J), again indicating an increased contribution of cellular senescence to the accelerated OA phenotype of *Trpc1*$^{-/-}$ mice post-DMM.

Discussion

Osteoarthritis is characterized by the progressive destruction of the articular cartilage accompanied by degenerative changes in surrounding joint tissues. However we currently are not able to fully understand the mechanistic stages linking early alterations in joint mechanics, inflammation, and cellular metabolism to the phenotypic changes typical of chondrocytes during osteoarthritis that have been demonstrated to drive tissue breakdown.

TRPC1 sits within the endoplasmic reticulum membrane and functions within the Ca^{2+} shuttling mechanism required by cells to refill the intracellular calcium stores that are emptied repeatedly during activation of both biochemical signaling and mechanically induced pathways. We have hypothesized that the cyclic nature of normal ambulatory movement, involving repeated loading and unloading events that induce shear and compressive stresses upon chondrocytes within the articular cartilage, require TRPC1 activity to sustain the refilling of intracellular calcium stores that are repeatedly cleared during stimulation. We have been able to demonstrate that TRPC1 is depleted during the early phases of OA development and that this loss of TRPC1 leads to failure of murine articular cartilage to maintain its homeostasis during the mechanical challenge provided by the destabilization of the medial meniscus model.

While initial expectations were that *TRPC1* could be downregulated at gene expression level following early inflammatory or mechanical stimulation as seen in previous *ex vivo* human datasets (23, 30), microarray data from previous murine studies do not indicate that *Trpc1* expression is modulated in this way within our examined species and time points (31, 32) (publicly available dataset GSE169077), which aligns with lack of downregulation at gene expression level in human OA patients (GSE114007) (19) . Instead, we can hypothesize that the reduction in TRPC1 protein levels evident in immunohistology analyses of both murine and human cartilage during OA

development may occur due to degradation or removal of the channels. Indeed, evidence of proteolytic degradation of the related TPRC5 and TRPC6 channels by calpain (33, 34), which is found within synovial fluid of OA patients (35), exists alongside the identification of TRPC1 as a substrate of caspase-11 within the control of NLRP3 inflammasome activation (36).

This study demonstrates the consequences of TRPC1 loss from chondrocytes, most clearly shown within the DMM model where genetic deletion resulted in an increased severity of OA-like cartilage degeneration 8 weeks following instability induction. Although the use of a chondrocyte-specific conditional mutant line would additionally eliminate any indirect effects of *Trpc1* deletion related to metabolic changes or systemic immune cell influence, no alterations in overall body weight, joint or cartilage structure were evident in either our newborn or age matched unchallenged mice, suggesting that TRPC1 plays no significant systemic role in either skeletal development or joint maturation. While other evidence from studies in skeletal muscle also show that sustained and repeated stimulation, in the form of muscle contraction during forced exercise, leads to functional failure as a consequence of an inability to refill intracellular stores sufficiently (18), our examination of cells obtained from *Trpc1*-deficient mice demonstrate that TRPC1 is required specifically in chondrocytes for the maintenance of phenotypic stability, the maintained expression of type II collagen and aggrecan and for protection against the development of a pathogenic senescent phenotype.

While significant phenotypic changes to chondrocytes are expected following DMM induction, Trpc1deficient mice exhibited an array of differential gene expression compared to wild type controls, as displayed in the RNA sequencing analysis. These data supported our immunostaining analyses that demonstrate that, at a time point of 2 weeks post DMM, while an increased number

of cells remain within the articular cartilage, they express markers of cellular senescence including $p16^{INK4a}$ and MMP13, display markers of irregular cell number homeostasis and have a low expression of stable chondrocyte markers. Our RNA sequencing DEGs do not significantly overlap with the senescence transcriptomic signature identified by Saul et al.(37)(SenMayo). This may firstly reflect the use in our study of a post-traumatic rather than an aging OA model, but also illustrates the incomplete senescence secretory phenotype exhibited by the *Trpc1*$^{-/-}$ chondrocytes. Similarly, other expected examples of senescence markers such as Cdkn1a were not found to be upregulated in our RNA sequencing, potentially as a consequence of our choice of timepoint for analysis.Our in vitro investigations into the effects of *Trpc1* deficiency on IL-1β induced cellular challenge demonstrate that while the increase in expression of specific SASPs such as CCL-2 is evident, this partial senescent phenotype is exacerbated by the failure of *Trpc1*$^{-/-}$ chondrocytes to undergo Ca^{2+} mediated caspase driven apoptosis. We see that *Trpc1*$^{-/-}$ cells, under conditions of challenge, fail to activate the physiological pathway leading to apoptosis and rather acquire a senescent-like 'zombie' phenotype, whereby they are unable to perform other homeostatic functions such as respond to FGF signaling (21). Previous studies have demonstrated the important role of SASPs in skin wound healing and in liver regeneration (38, 39), suggesting that the lack of a full SASP phenotype in *Trpc1*$^{-/-}$ mice post-DMM might actually be detrimental to any repair attempt within the cartilage. These factors likely contribute to the accelerated development of cartilage breakdown which results in the more severe phenotype in *Trpc1*-deficient mice that we observe 8 weeks post-DMM.

The accumulation of senescent cells during osteoarthritis has been shown to contribute to joint degradation via the secretion of pro-inflammatory factors including IL-6, IL-17 and IL-1β known as the senescence associated secretory profile (SASP) (40). Senolytic approaches aiming at removing these cells from cartilage have been shown to improve outcome within animal models of OA (41). Although not yet successful within so far limited human OA trials, the therapeutic targeting of senescence development, removal of senescent cells or inhibition of SASP related elements represent

key opportunities in the search for disease modifying OA treatments (42). The RNA sequencing data collected within this study reveals the transcriptional activity linking the disruption to the normal chondrocyte phenotype caused by the failure of chondrocytes to sufficiently maintain homeostatic calcium signaling to the eventual breakdown of the articular cartilage. These mechanisms may become targets for future translational studies aimed at limiting the effects of the loss of TRPC1 during OA development.

Mechanosensitive ion channels have been previously implicated within cartilage biology, where deletion of TRPV4 was observed to decreased OA related changes during aging (15), whilst PiIEZO-1 and PIEZO-2 have roles in response to injury (17), with inflammation driving an increase in PIEZO-1 that increases both basal and responsive intracellular calcium concentrations to provide a feed-forward loop within OA pathogenesis (43). Other channels that are demonstrated to participate within the signaling pathways of known homeostatic mechanisms, such as within CXCR2 signaling (44, 45) may also represent valuable druggable targets for phenotypic modulation of chondrocytes, however the role of TRPC1 and its loss during OA development gives us several strategies for therapeutic development that require evaluation. While agonists able to specifically activate this channel only are not yet available, we believe that the activation step may be secondary to the need to preserve, re-express and stabilize TRPC1 within the endoplasmic reticulum or to facilitate its translocation to the cell surface.

Methods

Sex as a biological variable

This study examined human cartilage tissue from both male and female patients, with no differences found between sexes. The murine study exclusively used male mice because male mice exhibited less variability in phenotype.

Human cartilage samples

Samples of knee cartilage were collected during implantation of total knee arthroplasty as well as in unicondylar joint replacement at the Department of Orthopaedic Surgery of the University Hospital Magdeburg. The study was reviewed and approved by the Institutional Review Board (IRB) of the Medical School, Otto-von-Guericke University, Magdeburg (IRB No: 28/20). The patients/participants provided their written informed consent to participate in this study. Details of the included patients can be found in Supplemental Table 2. OA severity was determined histologically using the OARSI Score. Knee cartilage from patients who had died without a history of OA was used as a control. The absence of OA was assessed histologically.

Mice

Trpc1^{tm1Lbi} mice within the C57BL/6J background, originally generated by Dietrich et al. (46) were used for all *in vitro* and *in vivo* TRPC1 knockout experiments. This mouse lacks exon 8, which sits within the transmembrane region of the channel, leading to a premature stop codon within the *trpc1* transcript. All mice were housed within ventilated cages in a 12-hour day/night cycle with food and water *ad libitum*. All animal experiments were approved by the local ethics committee ‘Landesamt

für Natür, Umwelt und Verbraucherschutz Nordrhein-Westfalen' (LANUV, 84.02.04.2017.A050 and 84-02.05.50.15.005) and were carried out in compliance with ARRIVE guidelines.

Destabilization of the medial meniscus (DMM) was carried out as described previously (3, 47) on 10 week old male *Trpc1*$^{-/-}$ mice and age- and sex-matched wild type controls from within the same C56BL7/6J breeding colony. Right knees were subjected to DMM, while a sham surgery was performed on the left knee of each mouse, where the skin and joint capsule were opened but no damage was caused to the cartilage or ligaments. Mice were euthanized at either 2 weeks or 8 weeks post-DMM and knee joints were collected for histological processing or RNA library construction.

Histology and immunostaining

Human and murine tissues were fixed in 4% paraformaldehyde overnight, dehydrated, embedded in paraffin and cut in 5 μm sections. Safranin-O staining (0.2%, pH4.2) was used for histological analysis of the articular cartilage. Stained sections were imaged using an Axiovert Z1 microscope (Zeiss, Germany) and osteoarthritis severity was assessed using the OARSI scoring system (48). Between 3 and 5 sections per samples spanning each human sample, or weight bearing area of the murine knee joint were scored by 2 independent scorers blinded to the experimental group.

For immunostaining of TRPC1 and of phenotypic markers, deparaffinized sections were rehydrated and subjected to pepsin (1100 U/ml in 0.02 % HCl) digestion for 45 mins at 37°C for antigen retrieval. Tissues were blocked in 20% fetal calf serum (FCS) in PBS with 0.2% Tween20 for 1 hour at room temperature. Sections were stained with antibodies as listed in Supplemental Table 3 and detected either via fluorescence microscopy or by DAB detection (Vector Labs, USA) and light microscopy using an Axiovert Z1 microscope (Zeiss, Germany) after mounting using Mowiol

(Sigma-Aldrich, Germany) on glass slides. Quantification was performed as stated in individual figures, either by the counting of individual positive cells normalized for area of interest using ImageJ (v.2.1), or by quantification of positive staining intensity using ImageJ. Analyses were conducted on between 3 and 5 individual sections per joint for each staining, with the mean value per animal used for statistical comparison. Only the articular cartilage of the tibial plateau and femoral condyles are included within analyses, as outlined within Figure 1I. Meniscus, subchondral bone, developing osteophytes and bone marrow are excluded.

Chondrocyte cell culture and stimulation

Primary articular chondrocytes were isolated from the knee joints of 4-6 day old mice as described previously (49) using 1 mg/ml Collagenase IV in complete medium (DMEM high glucose (Gibco, USA) containing 10% fetal calf serum superior (Biochrom GmbH, Germany), 1% sodium pyruvate (Gibco, Germany) and 1% penicillin/streptomycin (Sigma-Aldrich, Germany). Chondrocytes were used at 80% confluency for experiments within the first passage unless otherwise stated and stimulated with 10ng/ml of murine IL-1β (Preprotech, USA) where required.

Immunofluorescence staining of chondrocytes

Immunofluorescence staining for TRPC1 was performed to detect the localization of the channel within the cells. Chondrocytes were grown to 80% confluence on glass coverslips, fixed in 4% PFA for 10 minutes and washed twice with PBS. Cells were permeabilized with PBS-TritonX for 10 minutes and quenched with 0.025% ammonium chloride in PBS for two 5-minute washes. After blocking with 20% FCS in PBS for 1 hour at room temperature, cells were incubated with primary

and secondary antibodies as listed in Supplemental Table 3 and detected using fluorescence microscopy using an Axio Imager 2.0 with Apotome (Zeiss, Germany).

Immunoblotting

Cell lysates containing equal amounts of protein and loading dye were separated by electrophoresis on 10% SDS page gels (Biorad, USA) alongside PageRulerTM Plus prestained protein ladder (ThermoFisher, USA) at 80 V. Proteins were transferred to a nitrocellulose membrane using a Trans-blot Turbo system (Biorad, USA), blocked in BSA (5% in TBS-T) at room temperature for 3 hours and incubated overnight at 4°C with the primary antibody as listed in Supplemental Table 3, washed three times in TBS-T and incubated with HRP-linked secondary antibody for 1 hour at room temperature. Membranes were washed, incubated with ECL solution and visualized via chemiluminescence using a Fusion FX Western blot imager (Vilber Lourmat, Germany).

TUNEL staining

Cells undergoing cell death were detected using the *In situ* cell death detection kit, TMR red (Merck, Germany) according to the manufacturer's instructions. In brief, paraffin sections were deparaffinized, rehydrated and permeabilized. Sections were incubated with the TMR red label for broken DNA strands and counterstained using DAPI. After mounting in mowiol. staining was visualized using an Axiovert Z1 microscope (Zeiss, Germany). Sections pre-treated with DNase I (1 U) for 10 minutes were used as a positive control.

Quantitative real time PCR

Total RNA was extracted from chondrocyte cultures using TRIzol® (Invitrogen, USA) as previously described using chloroform separation and isopropanol and 70% ethanol washes. cDNA was synthesized using the Taqman™ Reverse Transcription kit (Invitrogen, USA) according to the manufacturers' instructions. 1000 ng of RNA was transcribed using oligo(dT)16-primers and relative 1'CT gene expression levels were analyzed using primer sequences or Taqman probes (ThermoFisher Scientific) listed in Supplemental Table 4 using a CFX384 qPCR cycler (Biorad, USA) and beta-2-microglobulin (B2m), actin beta (Actb) and glyceraldehyde 3-phosphate dehydrogenase (Gapdh) forming a housekeeping (HK) control gene panel.

RNA sequencing

Total RNA was extracted from femoral head and tibial cartilage and subchondral bone pooled from 2–3 mouse knees per sample (DMM-WT, n=3 and DMM-TRPC$^{-/-}$, n=4), was assessed for quality using an RNA Nano chip on a Bioanalyzer (Agilent, Santa Clara, CA, USA). Average RNA integrity number (RIN) for the 7 samples was 7.9 ± 1.7 SD. Samples were quantified using the Qubit RNA BR fluorometric assay (ThermoFisher) on the DS-11 spectrophotometer (Denovix, Wilmington, DE, USA). 300 ng total RNA of each sample was used to prepare sequencing libraries using the TruSeq Stranded Total RNA with RiboZero as per manufacturer's recommendations (Illumina, San Diego, CA, USA) and previously described (50). Library quality was assessed on a Bioanalyzer high sensitivity DNA chip. Average library size was 300 bp ± 9 bp SD. Seven libraries were volumetrically pooled and sequenced on an Illumina NextSeq 550 instrument for 75 paired- end read cycles at the Schroeder Arthritis Institute (Krembil, Toronto, ON, Canada).

Demultiplexing of samples was performed using bcl2fastq conversion tool (v2.19.1.403). Quality assessment of each sample revealed high quality of reads (90.4% >Q30; 80 ± 14 million reads/per

end). To maintain a minimum read length of 25 bp post trimming of adapters, Cutadapt (v2.5) software was executed (very few reads being contaminated ~3%) along with trimming of Ns. Splice-aware alignment of reads using a Hierarchical Graph FM index (HGFM) method was performed using HISAT2 software (v2.1.0 with parameters --rna-strandness RF –dta) against mouse reference genome (vGRCm38). To populate the abundance of transcripts based on the reference genome and transcriptome, StringTie (v2.0.3 with parameters -e -B -G referencetranscripts.gtf) was run to generate output as table format files. These files were processed using the script 'prepDE.py' from StringTie software to collect the raw gene expression levels for downstream processing.

Raw gene expression levels consisted of 55,401 genes measured across the 7 samples. After filtering for lowly expressed genes, defined as genes with <2 samples with a count per million ≤1 16,429 genes remained for further analysis. Changes in RNA-seq expression were evaluated using a method that assumes a negative binomial distribution (51). Differential expression analyses were performed using function DESeq (default parameters) in R package DESeq2 (52). Pairwise comparisons between groups of interest were calculated and tested for statistical differences in expression levels, visualized using a volcano plot created in R. The false discovery rate (FDR) correction was used to adjust p-values (53), where 5% identified statistically significant differentially expressed genes (DEGs). All analyses were performed in R (v3.5.0). DEGs were further represented using heatmap.2 function in gplots (v3.0.1). Gene Ontology biological process (BP) enrichment analysis was performed using clusterProfiler (v4.0.5 in R 4.1.0) and resulting plots were generated in R using ggplot (v2 3.3.5).

Intracellular calcium measurement

To measure the levels of intracellular Ca^{2+} mobilization, chondrocytes were seeded within a 96- well plate (30000 cells/well) and loaded with Fluo-4 reagent before stimulation according to the manufacturer's instructions. Cells were then monitored for fluorescence signal using the Axiowert A1 with live cell imaging CO_2 chamber and heating plate (Zeiss, Germany) under standard culture conditions. Basal levels were measured via fluorescence imaging using an excitation wavelength of 494nm and emission wavelength of 516nm, every 15 seconds for 2 minutes under resting conditions, before any stimulus was added. Following stimulation using a standardized 5 ul volume of either PBS, ionomycin, thapsigargin or bFGF, further measurements were taken every 15 seconds for 5 minutes. The change in fluorescence intensity was calculated relative to basal levels.

Senescence associated β-Galactosidase (SA-β-GAL) detection

β-galactosidase activity, a marker of cells undergoing senescence, was detected by cytochemical cleavage of the chromogenic substrate 5-bromo-4-chloro-3-indoyl β-D-galactopyranoside (X-Gal) into an insoluble compound at the pH of 6.0. Cells were fixed with glutaraldehyde/formaldehyde (0.2% / 2% in PBS), washed in PBS and covered with the X-Gal staining solution (54) for 20 hours at 37°C. Cells were then washed with methanol and air dried before imaging using an Axiovert Z1 microscope (Zeiss, Germany).

ELISA analyses

Protein concentrations within supernatant collected following 24 hours incubation with 10ng/ml IL-1β followed by 48 hours further culture in control medium were collected and used for ELISA quantification with the following kits according to the manufacturer's instructions: Mouse CCL2/JE/MCP-1 Quantikine ELISA (R&D Systems), Mouse IL-6 Quantikine ELISA (R&D Systems) and Mouse Total MMP-3 Quantikine ELISA (R&D Systems). Quantification was performed with reference to the standard solutions provided in each kit.

Proliferation assay

Chondrocyte proliferation was measured in vitro using the CyQUANT® Cell Proliferation Assay (ThermoFisher Scientific) according to the manufacturer's instructions, which uses a fluorescent nucleic acid dye to measure the DNA content within a sample. The proliferation rate was calculated by dividing the content measured after 48 hours incubation with either control or 10 ng/ml IL-1β with that measured after 24 hours incubation.

Caspase activity assay

Caspase activity as a measure of caspase mediated apoptosis was measured using the Generic Caspase Activity Assay Kit (Fluorometric – Green) (Abcam). Chondrocytes incubated with either control or 10 ng/ml IL-1β containing media for 24 hours followed by 48 hours further culture in control medium were labelled according to the manufacturer's instructions, before fixation in 4% paraformaldehyde and visualization using an Axiovert Z1 microscope (Zeiss, Germany).

MicroCT imaging and analysis

MicroCT scanning of knee joints was performed using a Skyscan 1176 scanner (Bruker, USA), with a 0.5 aluminium filter, 0.3° rotation with 10 images per step. Scans were reconstituted using NRecon (version 1.7.4.6) and images were positioned for quantitative analysis using DataViewer (Version 1.5.6.3) software. The tibial plateau was selected and analysed using CTAn (Version 1.1.8.9.0) software, where subchondral bone plate and subchondral bone trabecular parameters could be separated. Bone parameters analyzed included subchondral bone (SCB) thickness, bone volume fraction (BV/TV), trabecular thickness (Tb. Th.) and trabecular separation (Tb. Sp.).

Statistical analyses

Statistical analyses were performed using GraphPad Prism version (v9.0) software. Individual tests and statistical significance levels are indicated within figures and figure legends. Unless stated otherwise, data are presented as mean±SEM and p values < 0.05 were considered statistically significant. 2-tailed Student's t-test was used for statistical analysis unless otherwise stated in the figure legend.

Study approval

For human studies, written informed consent was received prior to sample donation. All human and murine studies were approved by the appropriate institutional review boards as described above.

Data Availability

All data relevant to the study are included in the article or uploaded as supplementary information, aside from RNA sequencing data that will be available in a public open access repository upon acceptance of the manuscript. Supporting data values associated with the main manuscript and supplemental material are available within the Supporting data values file.

Author Contributions

MS, SL: experimental design, data acquisition, data analysis and interpretation, writing of the manuscript. OEG, PPo, CP: data analysis and interpretation. JB: provision of human tissue samples. SB, LW, SK, PPa, RA, AS, JI: data acquisition. FDA: data analysis and interpretation, writing of the manuscript. MK: experimental design, data analysis and interpretation, writing of the manuscript. TP: conceptualization, experimental design, data analysis and interpretation, writing of the manuscript. JS: conceptualization, data acquisition, data analysis and interpretation, writing of the manuscript. All authors have edited and approved the manuscript.

Acknowledgements

This work was supported by funding from the ‘Bundesministerium für Bildung und Forschung’ (BMBF) (Project: 01EC1408F), ‘Deutsche Forschungsgemeinschaft‘ (DFG) (Grants: SH 832/4-1 and BE 4328/9-1), the ‘Innovative Medizinische Forschung’ (IMF) program of the University Hospital Münster (Projects I-SH121608 and I-SH112111) and from the Tony and Shari Fell Platinum Chair in Arthritis Research, University Health Network Foundation, Toronto, ON, Canada.

References

1. (OARSI) ORSI. Osteoarthritis: A serious disease. 2016.
2. Kloppenburg M, Berenbaum F. Osteoarthritis year in review 2019: epidemiology and therapy. Osteoarthritis Cartilage. 2020;28(3):242-8.
3. Sherwood J, Bertrand J, Nalesso G, Poulet B, Pitsillides A, Brandolini L, et al. A homeostatic function of CXCR2 signalling in articular cartilage. Ann Rheum Dis. 2015;74(12):2207-15.
4. Sherwood J. Osteoarthritis year in review 2018: biology. Osteoarthritis Cartilage. 2019;27(3):365-70.
5. Matta C, Takacs R, Ducza L, Ebeid RA, Choi H, Mobasheri A. Ion channels involved in inflammation and pain in osteoarthritis and related musculoskeletal disorders. Am J Physiol Cell Physiol. 2023;325(1):C257-C71.
6. Clapham DE. Calcium signaling. Cell. 2007;131:1047-58.
7. Zhou Y, Park M, Cheung E, Wang L, Lu XL. The effect of chemically defined medium on spontaneous calcium signaling of in situ chondrocytes during long-term culture. J Biomech. 2015;48(6):990-6.
8. Zhivotovsky B, Orrenius S. Calcium and cell death mechanisms: a perspective from the cell death community. Cell Calcium. 2011;50(3):211-21.
9. Lin SS, Tzeng BH, Lee KR, Smith RJ, Campbell KP, Chen CC. Cav3.2 T-type calcium channel is required for the NFAT-dependent Sox9 expression in tracheal cartilage. Proc Natl Acad Sci U S A. 2014;111(19):E1990-8.
10. Gawri R, Bielecki R, Salter EW, Zelinka A, Shiba T, Collingridge G, et al. The anabolic effect of inorganic polyphosphate on chondrocytes is mediated by calcium signalling. J Orthop Res. 2022;40(2):310-22.
11. Cheng KT, Liu X, Ong HL, Ambudkar IS. Functional requirement for Orai1 in store-operated TRPC1-STIM1 channels. J Biol Chem. 2008;283(19):12935-40.
12. Clapham DE. TRP channels as cellular sensors. Nature. 2003;426(6966):517-24.
13. Vincent TL, Wann AKT. Mechanoadaptation: articular cartilage through thick and thin. J Physiol. 2019;597(5):1271-81.
14. Li W, Zhou Y, Han L, Wang L, Lucas Lu X. Calcium signaling of primary chondrocytes and ATDC5 chondrogenic cells under osmotic stress and mechanical stimulation. J Biomech. 2022;145:111388.
15. O'Conor CJ, Ramalingam S, Zelenski NA, Benefield HC, Rigo I, Little D, et al. Cartilage-Specific Knockout of the Mechanosensory Ion Channel TRPV4 Decreases Age-Related Osteoarthritis. Scientific reports. 2016;6:29053-.
16. O'Conor CJ, Leddy HA, Benefield HC, Liedtke WB, Guilak F. TRPV4-mediated mechanotransduction regulates the metabolic response of chondrocytes to dynamic loading. Proc Natl Acad Sci U S A. 2014;111(4):1316-21.
17. Lee W, Leddy HA, Chen Y, Lee SH, Zelenski NA, McNulty AL, et al. Synergy between Piezo1 and Piezo2 channels confers high-strain mechanosensitivity to articular cartilage. Proc Natl Acad Sci U S A. 2014;111(47):E5114-22.
18. Zanou N, Shapovalov G, Louis M, Tajeddine N, Gallo C, Van Schoor M, et al. Role of TRPC1 channel in skeletal muscle function. Am J Physiol Cell Physiol. 2010;298(1):C149-62.
19. Fisch KM, Gamini R, Alvarez-Garcia O, Akagi R, Saito M, Muramatsu Y, et al. Identification of transcription factors responsible for dysregulated networks in human osteoarthritis cartilage by global gene expression analysis. Osteoarthritis Cartilage. 2018;26(11):1531-8.
20. Thastrup O, Cullen PJ, Drobak BK, Hanley MR, Dawson AP. Thapsigargin, a tumor promoter, discharges intracellular Ca2+ stores by specific inhibition of the endoplasmic reticulum Ca2(+)-ATPase. Proc Natl Acad Sci U S A. 1990;87(7):2466-70.
21. Vincent T, Hermansson M, Bolton M, Wait R, Saklatvala J. Basic FGF mediates an

immediate response of articular cartilage to mechanical injury. Proc Natl Acad Sci U S A. 2002;99(12):8259-64.
22. Ambudkar IS, de Souza LB, Ong HL. TRPC1, Orai1, and STIM1 in SOCE: Friends in tight spaces. Cell Calcium. 2017;63:33-9.
23. Dell'accio F, De Bari C, Eltawil NM, Vanhummelen P, Pitzalis C. Identification of the molecular response of articular cartilage to injury, by microarray screening: Wnt-16 expression and signaling after injury and in osteoarthritis. Arthritis & Rheumatism. 2008;58:1410-21.
24. Lefebvre V, Angelozzi M, Haseeb A. SOX9 in cartilage development and disease. Curr Opin Cell Biol. 2019;61:39-47.
25. Dell'Accio F, De Bari C, Luyten FP. Molecular markers predictive of the capacity of expanded human articular chondrocytes to form stable cartilage in vivo. Arthritis & Rheumatism. 2001;44:1608-19.
26. Ring NAR, Valdivieso K, Grillari J, Redl H, Ogrodnik M. The role of senescence in cellular plasticity: Lessons from regeneration and development and implications for age-related diseases. Dev Cell. 2022;57(9):1083-101.
27. Echtermeyer F, Bertrand J, Dreier R, Meinecke I, Neugebauer K, Fuerst M, et al. Syndecan-4 regulates ADAMTS-5 activation and cartilage breakdown in osteoarthritis. Nat Med. 2009;15:1072-6.
28. Goldring MB, Otero M. Inflammation in osteoarthritis. Current opinion in rheumatology. 2011;23(5):471-8.
29. Harr MW, Distelhorst CW. Apoptosis and autophagy: decoding calcium signals that mediate life or death. Cold Spring Harb Perspect Biol. 2010;2(10):a005579.
30. Comblain F, Dubuc JE, Lambert C, Sanchez C, Lesponne I, Serisier S, et al. Identification of Targets of a New Nutritional Mixture for Osteoarthritis Management Composed by Curcuminoids Extract, Hydrolyzed Collagen and Green Tea Extract. PLoS One. 2016;11(6):e0156902.
31. Bateman JF, Rowley L, Belluoccio D, Chan B, Bell K, Fosang AJ, et al. Transcriptomics of wild-type mice and mice lacking ADAMTS-5 activity identifies genes involved in osteoarthritis initiation and cartilage destruction. Arthritis Rheum. 2013;65(6):1547-60.
32. Loeser RF, Olex AL, McNulty MA, Carlson CS, Callahan M, Ferguson C, et al. Disease progression and phasic changes in gene expression in a mouse model of osteoarthritis. PLoS One. 2013;8(1):e54633.
33. Du W, Huang J, Yao H, Zhou K, Duan B, Wang Y. Inhibition of TRPC6 degradation suppresses ischemic brain damage in rats. J Clin Invest. 2010;120(10):3480-92.
34. Kaczmarek JS, Riccio A, Clapham DE. Calpain cleaves and activates the TRPC5 channel to participate in semaphorin 3A-induced neuronal growth cone collapse. Proc Natl Acad Sci U S A. 2012;109(20):7888-92.
35. Yamamoto S, Shimizu K, Shimizu K, Suzuki K, Nakagawa Y, Yamamuro T. Calcium-dependent cysteine proteinase (calpain) in human arthritic synovial joints. Arthritis Rheum. 1992;35(11):1309-17.
36. Py BF, Jin M, Desai BN, Penumaka A, Zhu H, Kober M, et al. Caspase-11 controls interleukin-1beta release through degradation of TRPC1. Cell Rep. 2014;6(6):1122-8.
37. Saul D, Kosinsky RL, Atkinson EJ, Doolittle ML, Zhang X, LeBrasseur NK, et al. A new gene set identifies senescent cells and predicts senescence-associated pathways across tissues. Nat Commun. 2022;13(1):4827.
38. Demaria M, Ohtani N, Youssef SA, Rodier F, Toussaint W, Mitchell JR, et al. An essential role for senescent cells in optimal wound healing through secretion of PDGF-AA. Dev Cell. 2014;31(6):722-33.
39. Cheng N, Kim KH, Lau LF. Senescent hepatic stellate cells promote liver regeneration through IL-6 and ligands of CXCR2. JCI Insight. 2022;7(14).
40. Coryell PR, Diekman BO, Loeser RF. Mechanisms and therapeutic implications of cellular senescence in osteoarthritis. Nat Rev Rheumatol. 2021;17(1):47-57.
41. Jeon OH, Kim C, Laberge RM, Demaria M, Rathod S, Vasserot AP, et al. Local clearance of

senescent cells attenuates the development of post-traumatic osteoarthritis and creates a pro-regenerative environment. Nat Med. 2017;23(6):775-81.
42. Diekman BO, Loeser RF. Aging and the emerging role of cellular senescence in osteoarthritis. Osteoarthritis Cartilage. 2024;32(4):365-71.
43. Lee W, Nims RJ, Savadipour A, Zhang Q, Leddy HA, Liu F, et al. Inflammatory signaling sensitizes Piezo1 mechanotransduction in articular chondrocytes as a pathogenic feed-forward mechanism in osteoarthritis. Proc Natl Acad Sci U S A. 2021;118(13).
44. Lindemann O, Umlauf D, Frank S, Schimmelpfennig S, Bertrand J, Pap T, et al. TRPC6 regulates CXCR2-mediated chemotaxis of murine neutrophils. Journal of immunology (Baltimore, Md : 1950). 2013;190(11):5496-505.
45. Lindemann O, Rossaint J, Najder K, Schimmelpfennig S, Hofschröer V, Wälte M, et al. Intravascular adhesion and recruitment of neutrophils in response to CXCL1 depends on their TRPC6 channels. Journal of Molecular Medicine. 2020;98(3):349-60.
46. Dietrich A, Kalwa H, Storch U, Mederos y Schnitzler M, Salanova B, Pinkenburg O, et al. Pressure-induced and store-operated cation influx in vascular smooth muscle cells is independent of TRPC1. Pflugers Arch. 2007;455(3):465-77.
47. Glasson SS, Askew R, Sheppard B, Carito B, Blanchet T, Ma H-L, et al. Deletion of active ADAMTS5 prevents cartilage degradation in a murine model of osteoarthritis. Nature. 2005;434(7033):644-8.
48. Glasson SS, Chambers MG, Van Den Berg WB, Little CB. The OARSI histopathology initiative - recommendations for histological assessments of osteoarthritis in the mouse. Osteoarthritis Cartilage. 2010;18 Suppl 3:S17-23.
49. Gosset M, Berenbaum F, Thirion S, Jacques C. Primary culture and phenotyping of murine chondrocytes. Nat Protoc. 2008;3(8):1253-60.
50. Tavallaee G, Lively S, Rockel JS, Ali SA, Im M, Sarda C, et al. Contribution of MicroRNA-27b-3p to Synovial Fibrotic Responses in Knee Osteoarthritis. Arthritis Rheumatol. 2022;74(12):1928-42.
51. Anders S, Huber W. Differential expression analysis for sequence count data. Genome Biol. 2010;11(10):R106.
52. Love MI, Huber W, Anders S. Moderated estimation of fold change and dispersion for RNA-seq data with DESeq2. Genome Biol. 2014;15(12):550.
53. Benjamini Y, Hochberg Y. Controlling the False Discovery Rate: A Practical and Powerful Approach to Multiple Testing. Journal of the Royal Statistical Society Series B (Methodological). 1995;57(1):289-300.
54. Debacq-Chainiaux F, Erusalimsky JD, Campisi J, Toussaint O. Protocols to detect senescence-associated beta-galactosidase (SA-betagal) activity, a biomarker of senescent cells in culture and in vivo. Nat Protoc. 2009;4(12):1798-806.

Figures and figure legends

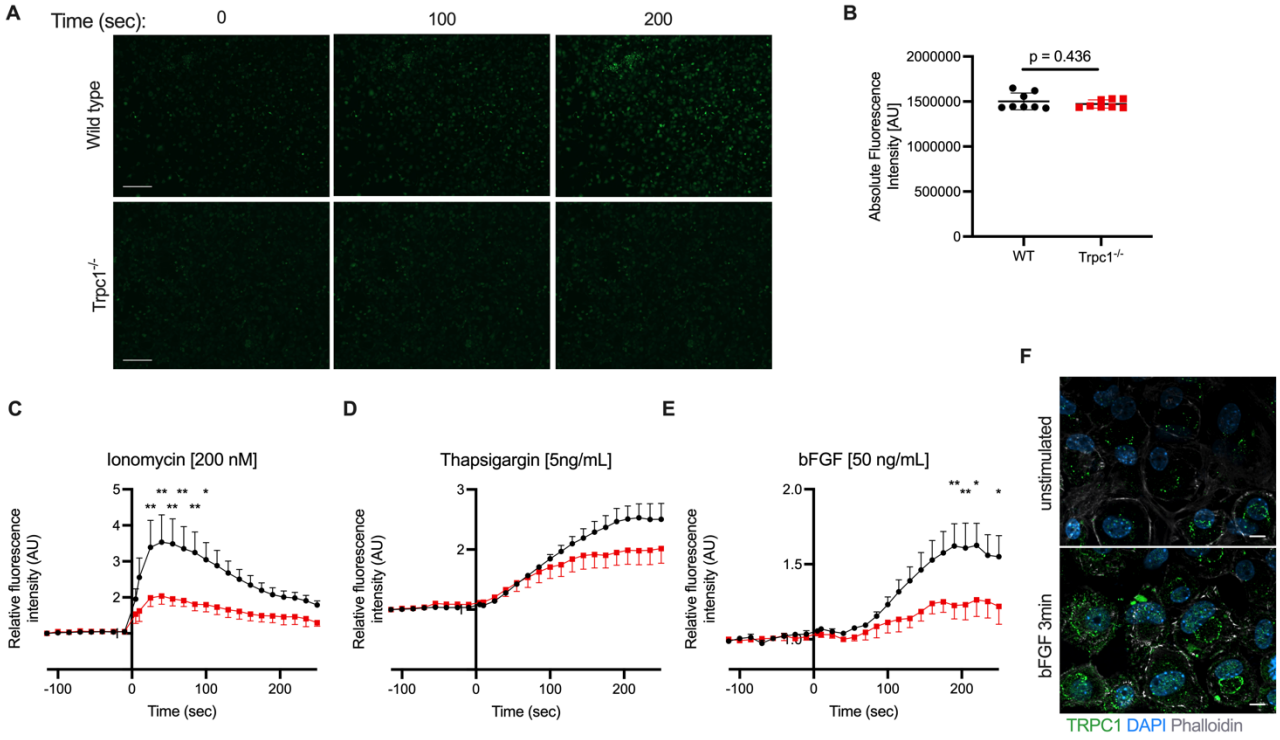

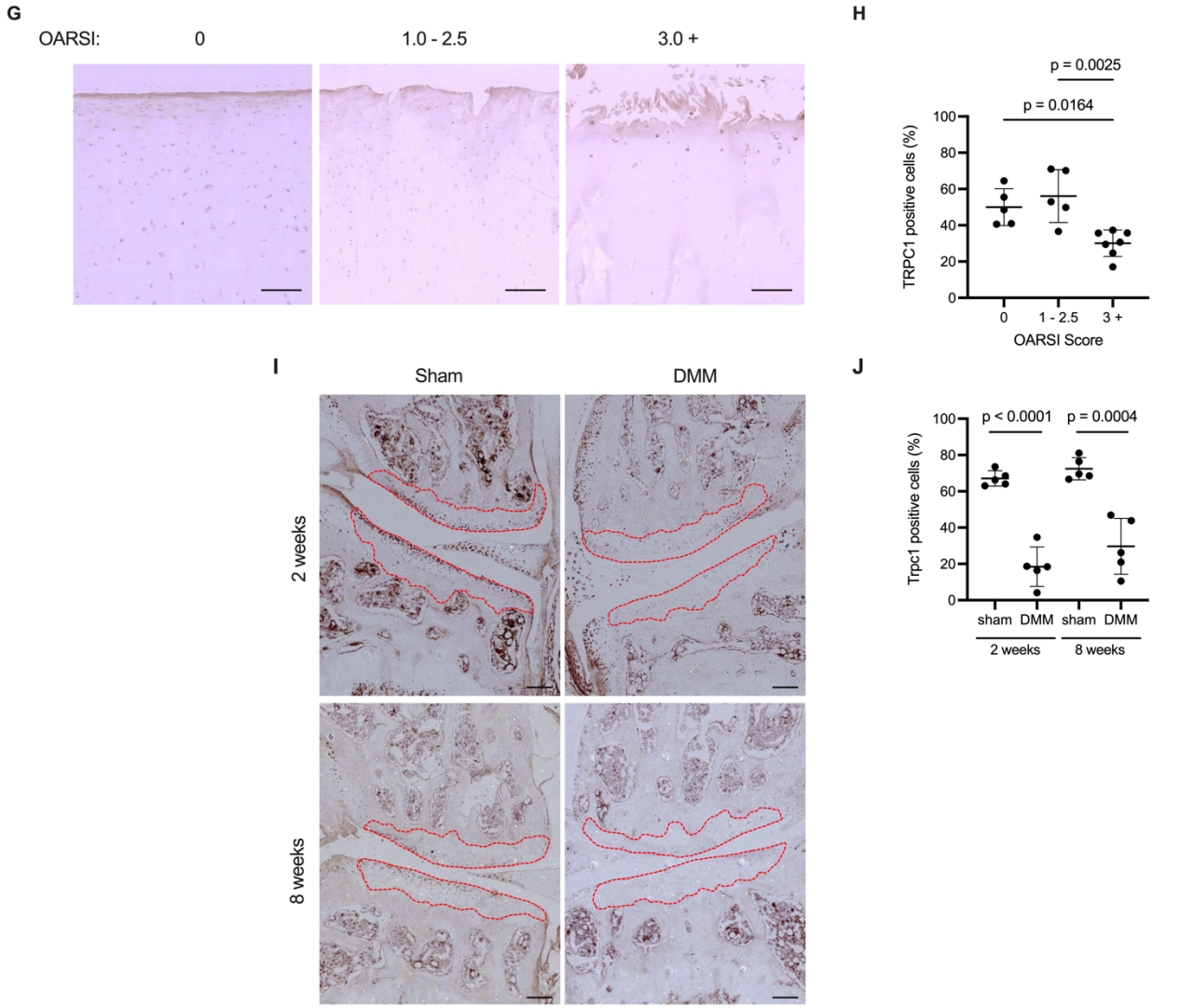

Figure 1

Analysis of TRPC1 protein expression in human and murine articular cartilage. (A) Fluorescence images depicting intracellular Ca^{2+} (green) within early passage wild type and TRPC1$^{-/-}$ chondrocytes loaded with Fluo-4 Ca^{2+} indicator, during stimulation with 5ng/ml thapsigargin. Scale bar: 200µm. (B) Comparison of basal intracellular Ca^{2+} levels as measured by fluorescence intensity of early passage wild type and *Trpc1*$^{-/-}$ chondrocytes. P values: unpaired t-test (n = 8). (C-E) Timecourse analysis of intracellular Ca^{2+} levels as measured by fluorescence intensity of loaded Fluo-4 Ca^{2+} indicator in wild type and *Trpc1*$^{-/-}$ chondrocytes during stimulation with either ionomycin (200nM), thapsigargin (5ng/ml) or bFGF (50ng/ml). P values: 2-way ANOVA with multiple comparisons (n = 4). *p<0.05 and **p<0.01. (F) Immunofluorescent detection of TRPC1 (green) in wild type murine chondrocytes in resting conditions and 3 mins following bFGF (50ng/ml) stimulation. Cell cytoskeleton is counterstained with phalloidin (white) and nuclei with DAPI (blue). Scale bar:20 µm. For isotype negative control staining, see Supplemental Figure 3A. (G) Immunohistological detection of TRPC1 in human cartilage sections comparing healthy (OARSI score 0), early OA (OARSI score 1.0–2.5) and advanced OA (OARSI score 3.0+). Scale bar:100µm. For isotype negative control staining, see Supplemental Figure 3B. (H) Graph showing quantification of TRPC1 positive cells within the cartilage expressed as percentage of total number of cells identified (n = 4 participants) P values: 1-way ANOVA with multiple comparisons test. (I) Immunohistological detection of TRPC1 in murine knee joint 2 weeks and 8 weeks following sham control or DMM surgery. Dotted red outline indicates area used for analysis of articular cartilage. Scale bar:100µm. For isotype negative control staining, see Supplemental Figure 3C. (J) Quantification of the relative number of TRPC1 positive cells within the tibial articular cartilage expressed as a percentage of cells present P values: unpaired t-test (n = 5 mic

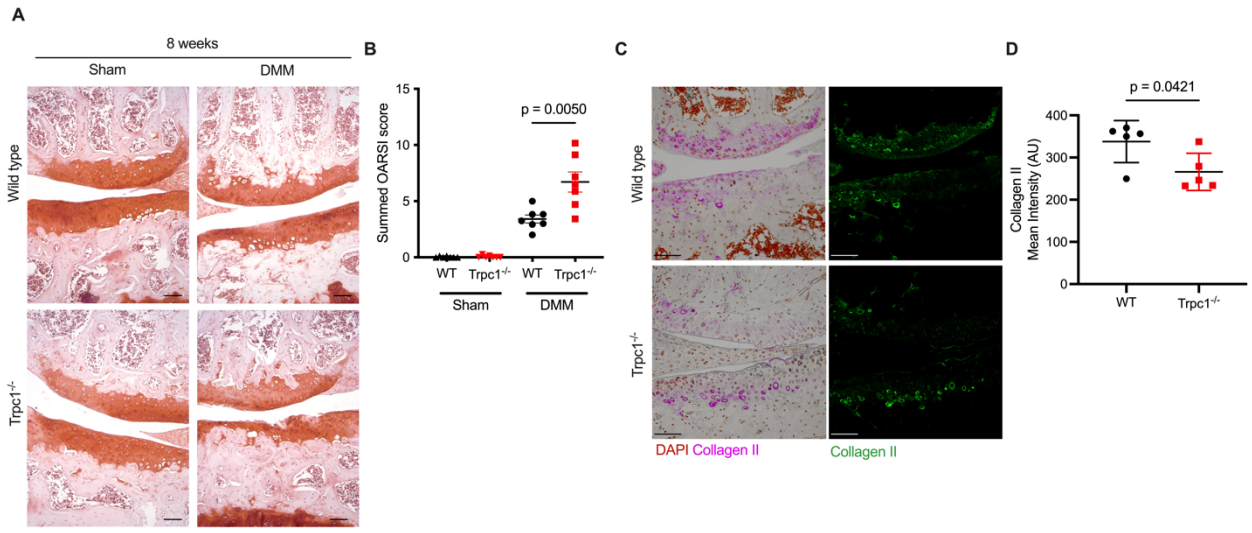

Figure 2

Assessment of articular cartilage phenotype 8 weeks post-surgery (sham vs DMM). (A) Representative images of Safranin-O stained paraffin sections of medial compartments of knee joints of wild type control and *Trpc1*$^{-/-}$ mice 8 weeks post-DMM. Scale bar:100 µm. (B) Summed OARSI score of medial and lateral compartments of wild type and Trpc1$^{-/-}$ knee joints 8 weeks post-DMM (n = 7). (C) Immunofluorescent detection of collagen type II in the medial compartments of wild type and *Trpc1*$^{-/-}$ knee joints 8 weeks post-DMM. Scale bar:100 µm. For isotype negative control staining, see Supplemental Figure 3D. (D) Quantification of the mean fluorescent signal intensity of collagen type II immunofluorescence within the remaining medial articular cartilage (n = 5). For all graphs, data expressed as mean ± SEM and P values determined by unpaired t-test.

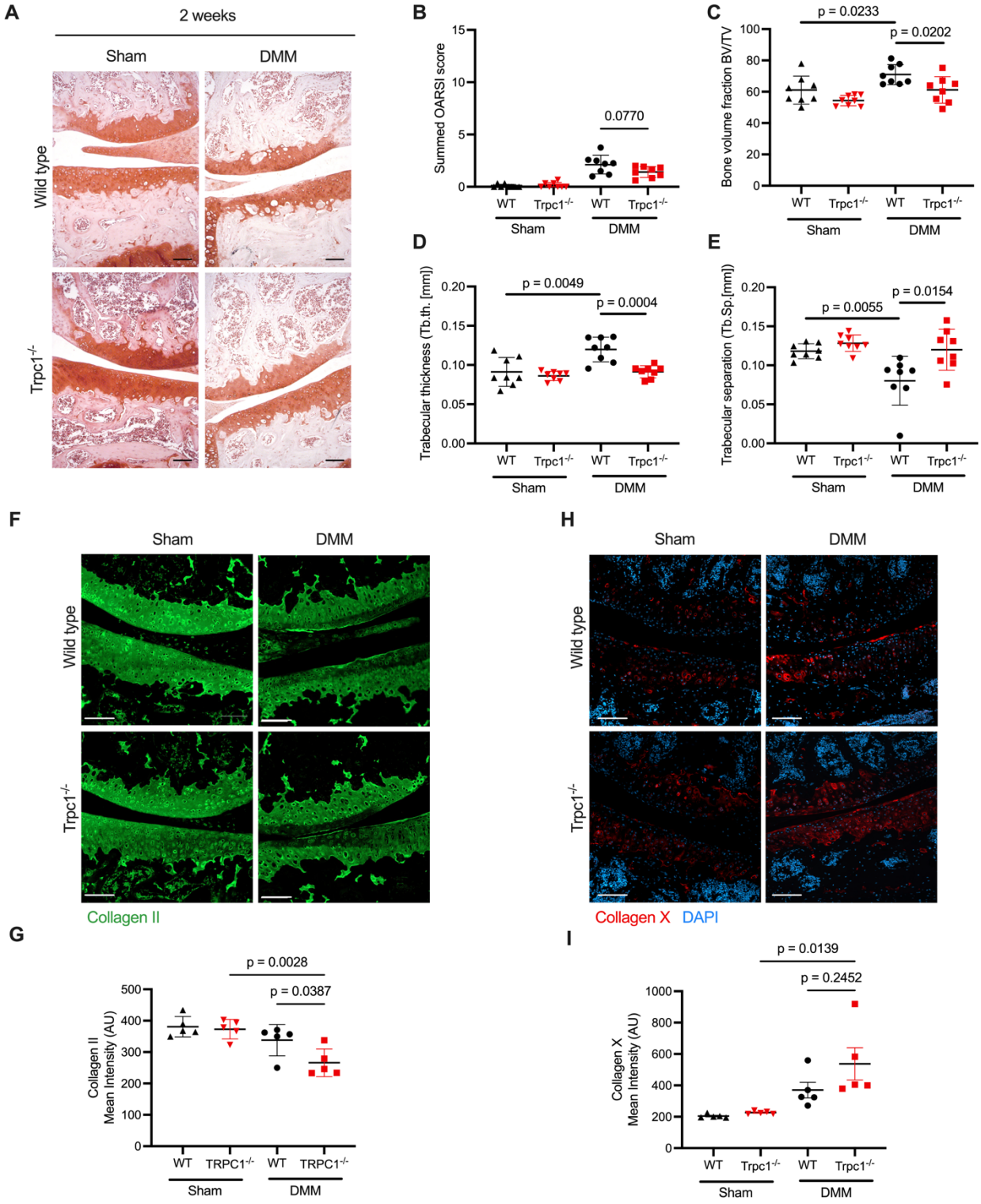

Figure 3

Assessment of early cartilage and subchondral bone changes 2 weeks post-DMM. (A) Representative images of Safranin-O stained paraffin sections of medial compartments of knee joints of wild type control and *Trpc1*$^{-/-}$ mice 2 weeks post-surgery (sham vs DMM). Scale bar: 100 µm. (B) Summed

OARSI score of medial and lateral compartments of wild type and *Trpc1*$^{-/-}$ knee joints 2 weeks post-DMM (n = 8). (C) Bone volume fraction (normalized for total volume; BV/TV) fraction measurement of wild type and *Trpc1*$^{-/-}$ knee joint tibial subchondral bone 2 weeks after sham control or DMM (n = 8). (D) Trabecular thickness (Tb.th. [mm]) measurement of wild type and *Trpc1*$^{-/-}$ knee joint tibial subchondral bone 2 weeks after sham control or DMM surgery (n = 8). (E) Trabecular separation (Tb.Sp. [mm]) in wild type and *Trpc1*$^{-/-}$ knee joint tibial subchondral bone 2 weeks after sham control or DMM (n = 8). (F) Immunofluorescent detection of collagen type II (green) in the medial compartments of wild type and *Trpc1*$^{-/-}$ knee joints 2 weeks post- DMM. Scale bar: 100 μm. For isotype negative control staining, see Supplemental Figure 3D. (G) Quantification of the mean fluorescent signal intensity of collagen type II immunofluorescence within the medial articular cartilage (n = 5) P values: 1-Way ANOVA with Tukey's multiple comparisons. (H) Immunofluorescent detection of collagen type X (red) in the medial compartments of wild type and *Trpc1*$^{-/-}$ knee joints 2 weeks post-DMM. Scale bar: 100 μm. For isotype negative control staining, see Supplemental Figure 3E. (I) Quantification of the mean fluorescent signal intensity of collagen type X immunofluorescence within the medial articular cartilage (n = 5) P values: 1-Way ANOVA with Tukey's multiple comparisons. For all graphs, data expressed as mean ± SEM and P values determined by unpaired t-test unless stated otherwise.

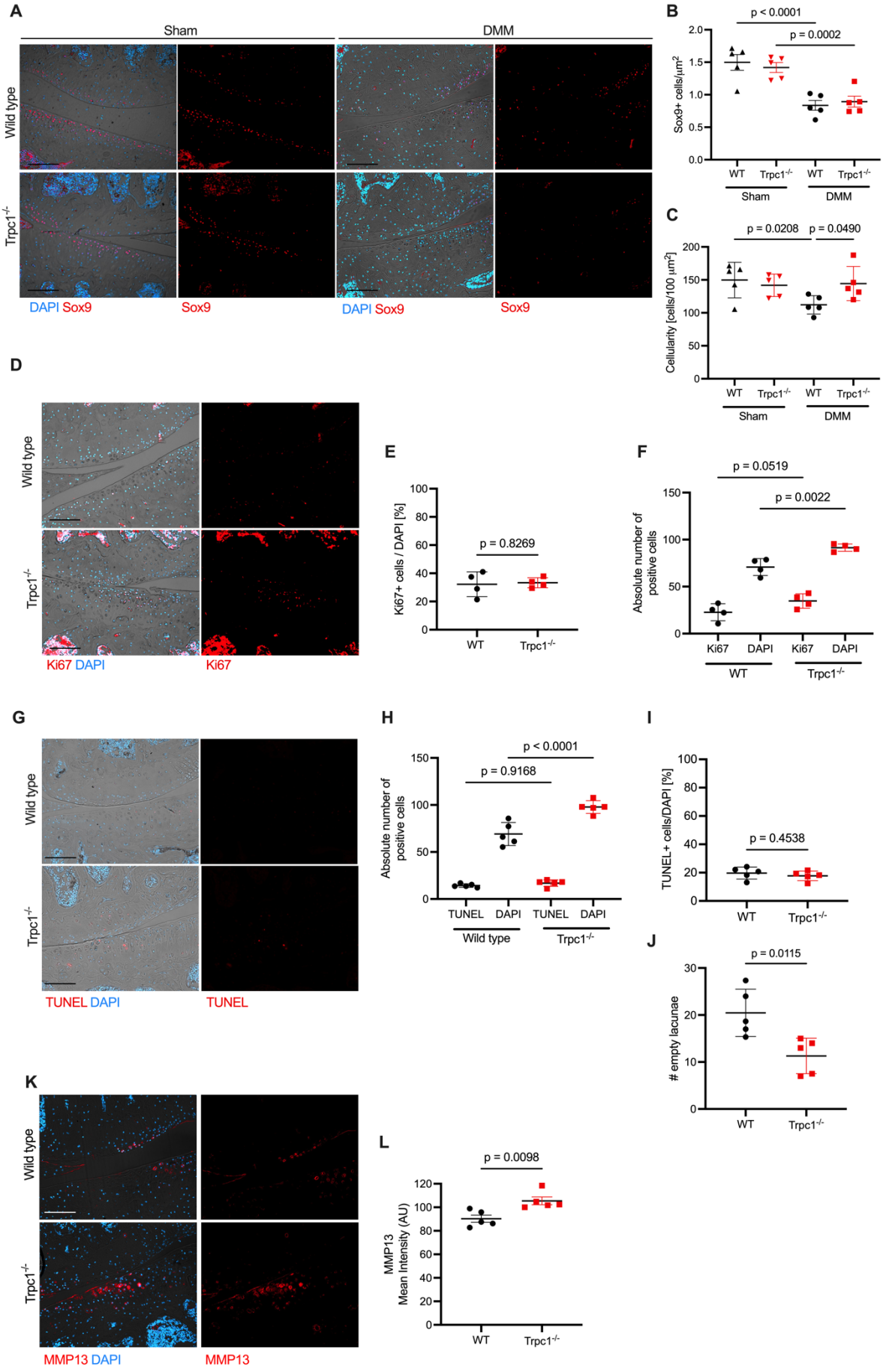
A
Sham
DMM
Wild type
Trpc1-/-
DAPI Sox9
Sox9
DAPI Sox9
Sox9
B
p < 0.0001
p = 0.0002
Sox9+ cells/µm2
WT
Trpc1-/-
WT
Trpc1-/-
Sham
DMM
C
p = 0.0208
p = 0.0490
Cellularity [cells/100 µm2]
WT
Trpc1-/-
WT
Trpc1-/-
Sham
DMM
D
Wild type
Trpc1-/-
Ki67 DAPI
Ki67
E
p = 0.8269
Ki67+ cells / DAPI [%]
WT
Trpc1-/-
F
p = 0.0519
p = 0.0022
Absolute number of positive cells
Ki67
DAPI
Ki67
DAPI
WT
Trpc1-/-
G
Wild type
Trpc1-/-
TUNEL DAPI
TUNEL
H
p < 0.0001
p = 0.9168
Absolute number of positive cells
TUNEL
DAPI
TUNEL
DAPI
Wild type
Trpc1-/-
I
p = 0.4538
TUNEL+ cells/DAPI [%]
WT
Trpc1-/-
J
p = 0.0115
# empty lacunae
WT
Trpc1-/-
K
Wild type
Trpc1-/-
MMP13 DAPI
MMP13
L
p = 0.0098
MMP13 Mean Intensity (AU)
WT
Trpc1-/-

Figure 4

TRPC1 dependent phenotypic changes in cartilage during early stages of OA development in mice. (A) Immunofluorescent detection of Sox9 in the medial compartments of wild type and *Trpc1*$^{-/-}$ knee joints 2 weeks post-DMM. DAPI used as a nuclear counterstain. (B) Quantification of density of Sox9^{+} cells within the medial tibial articular cartilage. P values: 1-Way ANOVA with Tukey's multiple comparisons. (n = 5). (C) Comparison of overall cellularity of medial tibial articular cartilage in wild type and *Trpc1*$^{-/-}$ 2 week post-DMM and sham mice as defined by number of DAPI^{+} cells per 100 μm^{2}. P values: 1-Way ANOVA with Tukey's multiple comparisons. (n=5). (D) Immunofluorescent detection of Ki67 as a marker of cell proliferation in medial compartments of murine knee joints 2 weeks post-DMM. DAPI used as a nuclear counterstain. (E) Quantification of number of Ki67^{+} cells within the medial tibial articular cartilage normalized for the total number of DAPI^{+} cells. P values: unpaired t-test (n = 4). (F) Absolute quantification of the number of Ki67^{+} cells and number of DAPI^{+} cells within the medial tibial articular cartilage 2 weeks post-DMM. P values: 1-Way ANOVA with Tukey's multiple comparisons (n=4). (G) TUNEL staining of medial compartments of murine knee joints 2 weeks post-DMM. DAPI used as a nuclear counterstain.
(H) Quantification of number of TUNEL^{+} cells normalized for total number of cells within the tibial articular cartilage. P values: 1-Way ANOVA with Tukey's multiple comparisons (n=5). (I) Absolute numbers of TUNEL^{+} and DAPI^{+} cells within the tibial articular cartilage 2 weeks post-DMM. (J) Quantification of number of empty lacunae within the tibial articular cartilage 2 weeks post-DMM. (K) Immunofluorescent detection of MMP-13 in medial compartments of wild type and *Trpc1*$^{-/-}$ knee joints 2 weeks post-DMM. DAPI used as a nuclei counterstain. (L) Quantification of mean MMP-13 staining intensity. P values: unpaired t-test (n = 5) unless stated otherwise. Scale bars: 100μm. For isotype negative control stainings, see Supplemental Figure 3.

A

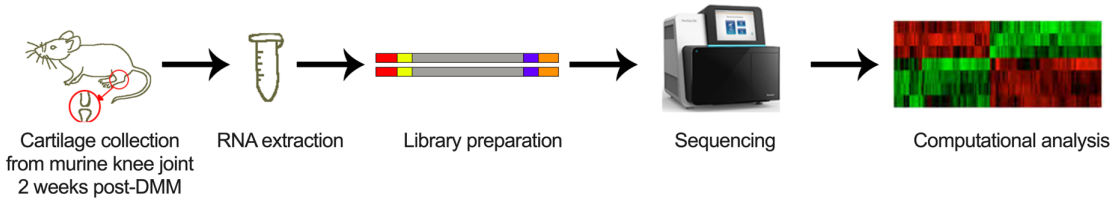
Cartilage collection from murine knee joint 2 weeks post-DMM
RNA extraction
Library preparation
Sequencing
Computational analysis

B

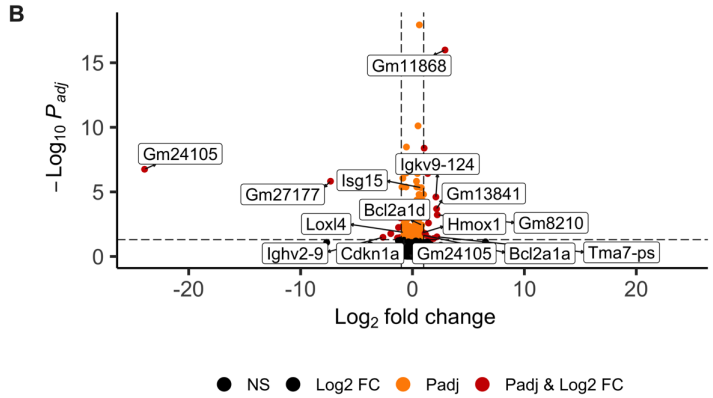
−Log10 Padj
Log2 fold change
Gm11868
Gm24105
Igkv9-124
Isg15
Gm27177
Gm13841
Bcl2a1d
Loxl4
Hmox1
Gm8210
Ighv2-9
Cdkn1a
Gm24105
Bcl2a1a
Tma7-ps
NS
Log2 FC
Padj
Padj & Log2 FC

C

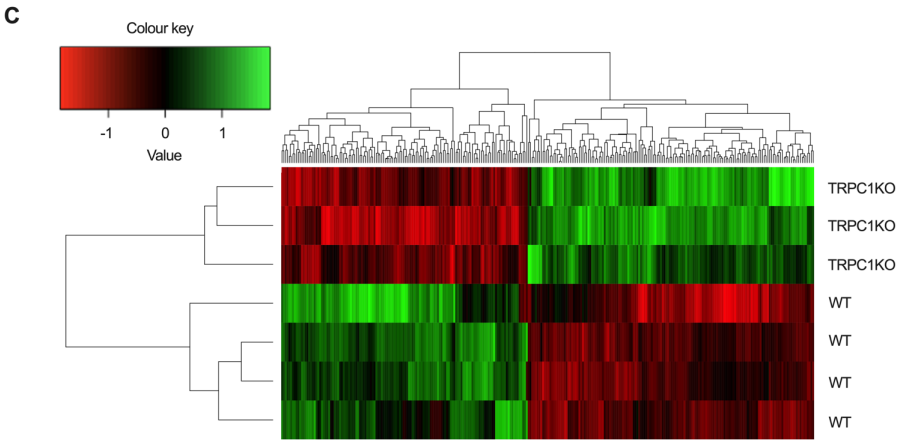
Colour key
Value
TRPC1KO
TRPC1KO
TRPC1KO
WT
WT
WT
WT

D

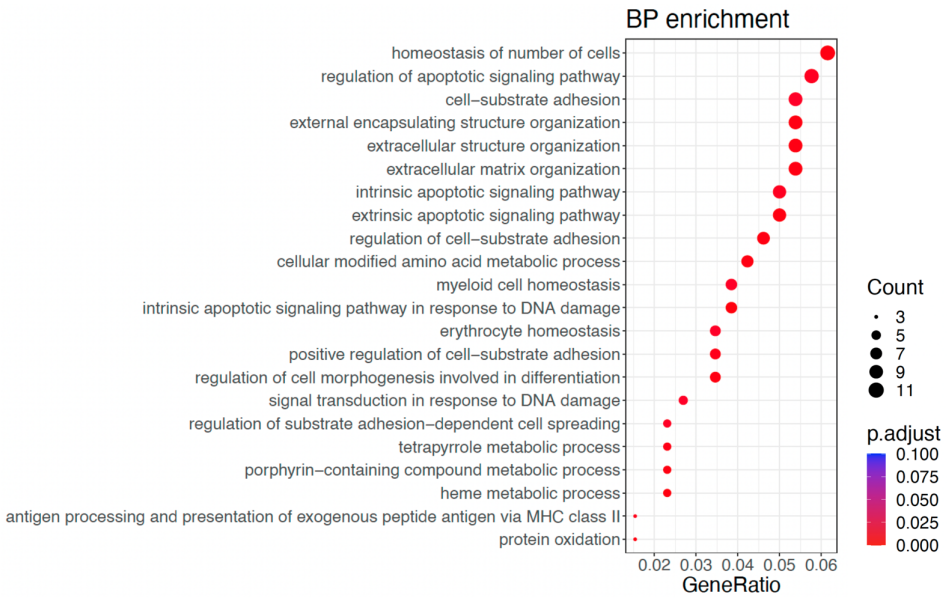
BP enrichment
homeostasis of number of cells
regulation of apoptotic signaling pathway
cell–substrate adhesion
external encapsulating structure organization
extracellular structure organization
extracellular matrix organization
intrinsic apoptotic signaling pathway
extrinsic apoptotic signaling pathway
regulation of cell–substrate adhesion
cellular modified amino acid metabolic process
myeloid cell homeostasis
intrinsic apoptotic signaling pathway in response to DNA damage
erythrocyte homeostasis
positive regulation of cell–substrate adhesion
regulation of cell morphogenesis involved in differentiation
signal transduction in response to DNA damage
regulation of substrate adhesion–dependent cell spreading
tetrapyrrole metabolic process
porphyrin–containing compound metabolic process
heme metabolic process
antigen processing and presentation of exogenous peptide antigen via MHC class II
protein oxidation
0.02 0.03 0.04 0.05 0.06
GeneRatio
Count
3
5
7
9
11
p.adjust
0.100
0.075
0.050
0.025
0.000

Figure 5

RNA expression profiles show an altered response to DMM in cartilage and subchondral bone. (A) Diagram of RNA sequencing workflow. (B) Volcano plot of cartilage gene expression fold-changes (FC, log2 scale) in *Trpc1*$^{-/-}$ relative to wild type mice 2 weeks after DMM and corresponding FDR-adjusted p-values P_{adj},-log10 scale). Dashed lines delineate cut-off values (BH-FDR, 0.05; FC, 1.5) and red dots highlight significantly differentially expressed genes (DEGs) (i.e., FC > 1.5 with P_{adj} < 0.05). (C) Heatmap showing DEG profiles (genes with FC > 1.5) in the individual samples from both *Trpc1*$^{-/-}$ and wild type groups, where green is upregulation and red is downregulation. (D) Biological pathway (BP) enrichment dotplot where gene ratio on the x-axis represents the ratio of the total DEGs in the given GO term on the y-axis. The size of each dot symbolizes the number of DEGs annotated with a specific term.

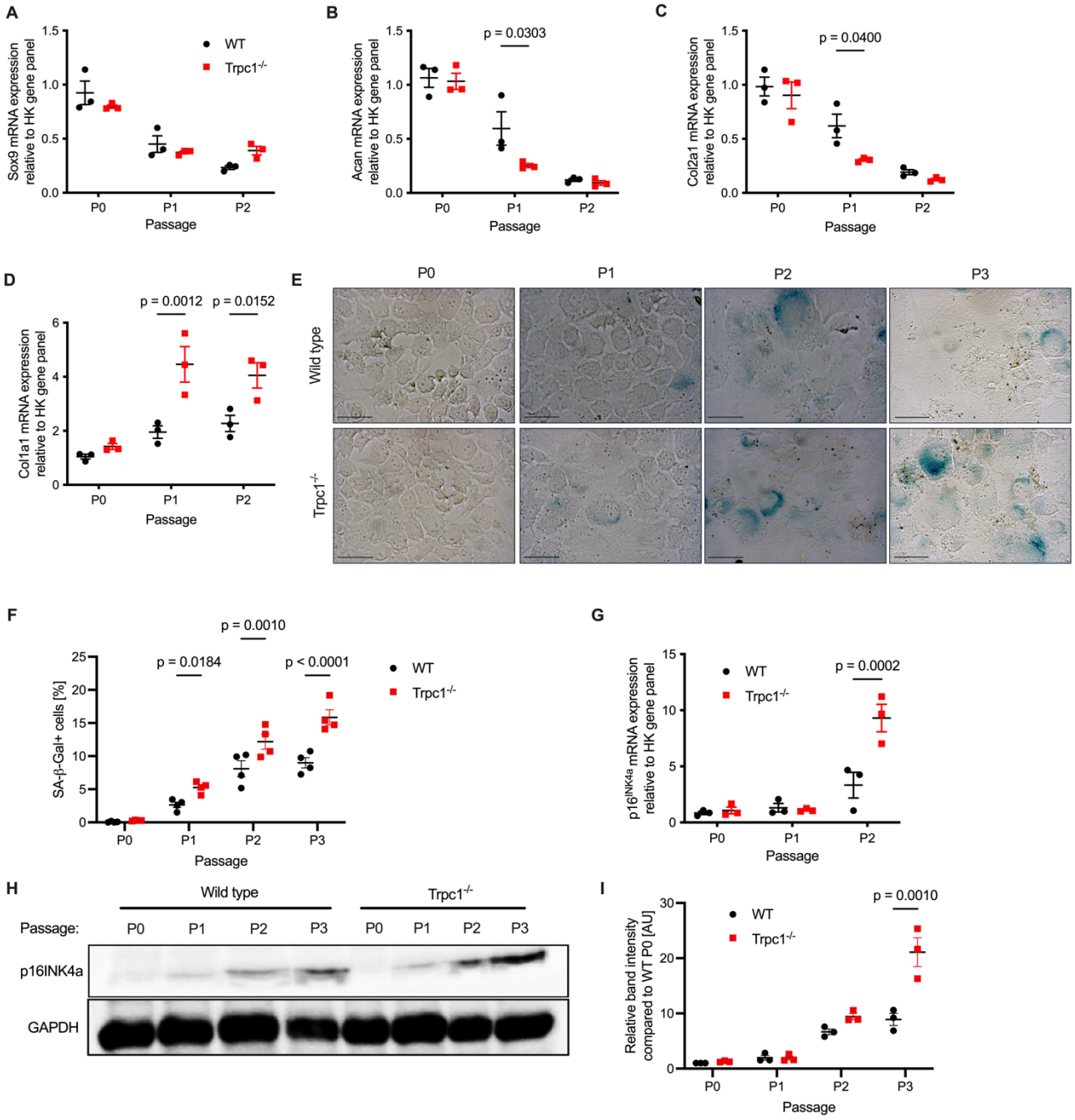

Figure 6

In vitro analysis of the effect of *Trpc1* deficiency upon chondrocyte phenotypic stability. (A-D) Real time RT-PCR analysis of *sox9*, aggrecan, *col2a1* and *col10a1* gene expression in murine wild type and *Trpc1*$^{-/-}$ chondrocytes during serial *in vitro* passage. P values: 2-way Anova with multiple comparisons (n = 3). (L) Representative images of SA-β-Gal staining (blue colour) of wild type and *Trpc1*$^{-/-}$ chondrocytes at equivalent confluence, visible by DIC counterimage, during serial passage.

Scale bar 50 μm. (M) Quantification of number of SA-β-Gal^{+} cells normalized for total number of cells during wild type and *Trpc1*$^{-/-}$ chondrocytes during serial passage. P values: 2-way ANOVA with multiple comparisons (n = 4, 20 images per condition). (N) Real time RT-PCR analysis of *p16INK4a* gene expression in wild type and Trpc1$^{-/-}$ chondrocytes during serial passage. P values: 2-way ANOVA with multiple comparisons (n = 3). (O) Western blot of p16^{INK4a} protein levels in wild type and *Trpc1*$^{-/-}$ chondrocytes during serial passage. GAPDH used as a loading control. (P) Quantification of Western blotting for p16^{INK4a} in wild type and *Trpc1*$^{-/-}$ chondrocytes during serial passage. P values: 2-way ANOVA with multiple comparisons (n = 3).

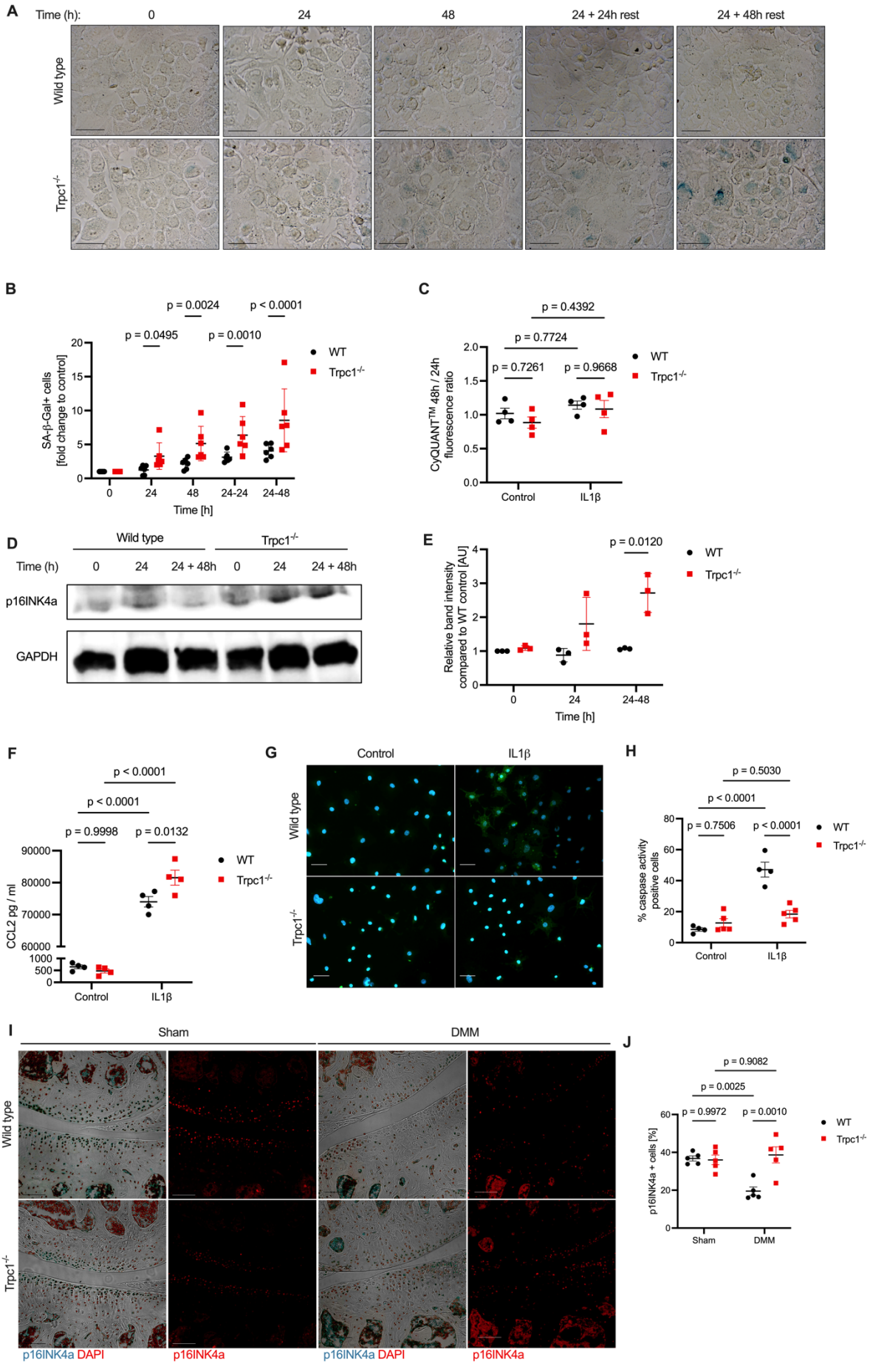
A
Time (h):
0
24
48
24 + 24h rest
24 + 48h rest
Wild type
Trpc1-/-
B
p = 0.0024
p < 0.0001
p = 0.0495
p = 0.0010
SA-β-Gal+ cells [fold change to control]
WT
Trpc1-/-
Time [h]
C
p = 0.4392
p = 0.7724
p = 0.7261
p = 0.9668
CyQUANT™ 48h / 24h fluorescence ratio
Control
IL1β
D
Wild type
Trpc1-/-
Time (h)
p16INK4a
GAPDH
E
p = 0.0120
Relative band intensity compared to WT control [AU]
F
p < 0.0001
p < 0.0001
p = 0.9998
p = 0.0132
CCL2 pg / ml
G
Control
IL1β
H
p = 0.5030
p < 0.0001
p = 0.7506
p < 0.0001
% caspase activity positive cells
I
Sham
DMM
p16INK4a DAPI
p16INK4a
J
p = 0.9082
p = 0.0025
p = 0.9972
p = 0.0010
p16INK4a + cells [%]

Figure 7

TRPC1 is required for protection against cellular senescence driven by IL-1β and during murine OA development. (A) Representative images of SA-β-Gal stainings (blue colour) of P0 wild type and *Trpc1*$^{-/-}$ chondrocytes treated with 10 ng/ml IL-1β for either 24 hours, 48 hours, or for 24 hours followed by an additional 24 or 48 hours culture in control medium (rest). (B) Quantification of number of SA-β-Gal^{+} cells normalized to those in control untreated samples (n = 5). (C) CyQUANT® fluorescence quantification of wild type and *Trpc1*$^{-/-}$ chondrocytes measured at 24 and 48hours post IL-1β stimulation to give a ratio representing proliferation rate (n = 4). (D) Western blot of p16^{INK4a} protein levels in wild type and *Trpc1*$^{-/-}$ chondrocytes treated with 10 ng/ml IL-1β for either 24 hours or for 24 hours followed by 48 hours culture in control medium. (E) Quantification of Western blotting for p16^{INK4a} in wild type and *Trpc1*$^{-/-}$ chondrocytes treated with 10 ng/ml IL-1β for either 24 hours or for 24 hours followed by 48 hours culture in control medium (n = 3). (F) CCL-2 concentration of control and IL-1β treated chondrocyte supernatants measured by ELISA (n = 4). (G) Representative images of cleaved caspase activity in chondrocytes treated with IL-1β for 24hrs plus 48hrs rest. (H) Quantification of cleaved caspase activity in wild type and *Trpc1*$^{-/-}$ chondrocytes following IL-1β stimulation (WT n = 4, *Trpc1*$^{-/-}$ n = 5). (I) Immunofluorescent detection of p16^{INK4a} in medial compartments of wild type and Trpc1$^{-/-}$ murine knee joints 2 weeks post-DMM. DAPI used as a nuclear counterstain. Scale bar: 100μm. For isotype negative control staining, see Supplemental Figure 3I. (J) Quantification of number of p16^{INK4a+} cells within the medial articular cartilage normalized for the total number of DAPI^{+} cells (n = 5). P values: 2-way ANOVA with multiple comparisons.